

DEMETER — Soft X-Ray Micro-Spectroscopy Beamline at NRSC SOLARIS and Its Performance in the Study of Magnetic Materials

A. MANDZIAK^{a,*}, K. MATLAK^a, B. WOLANIN^a, P. NITA^b, T. STRĄCZEK^a,
M. ZAJĄC^a, N. SPIRIDIS^c, J. KORECKI^c, D. WILGOCKA-ŚLĘZAK^c,
E. MADEJ^c AND T. TYLISZCZAK^a

^a*National Synchrotron Radiation Centre (NRSC) SOLARIS, Jagiellonian University, Czerwone Maki 98, 30-392 Kraków, Poland*

^b*Faculty of Physics, Astronomy and Applied Computer Science, Jagiellonian University, prof. Stanisława Łojasiewicza 11, 30-348 Kraków, Poland*

^c*Jerzy Haber Institute of Catalysis and Surface Chemistry Polish Academy of Sciences, Niezapominajek 8, 30-239 Kraków, Poland*

Received: 16.12.2025 & Accepted: 08.04.2026

Doi: [10.12693/APhysPolA.149.S174](https://doi.org/10.12693/APhysPolA.149.S174)

*e-mail: anna.mandziak@uj.edu.pl

DEMETER is a soft X-ray beamline at the SOLARIS National Synchrotron Radiation Centre, designed for high-resolution studies of magnetic materials using tunable, variable-polarization radiation in the 100–2000 eV range generated by an elliptically polarizing undulator. The beamline consists of two complementary end-stations, i.e., (i) a spectroscopic photoemission and low-energy electron microscope, and (ii) a scanning transmission X-ray microscope. The capabilities of the beamline are demonstrated through studies of X-ray magnetic circular and linear dichroism in NiO layers grown on Fe₃O₄, revealing element-specific magnetic contrast and interfacial coupling. Furthermore, investigations of strontium hexaferrite nanostructures using a scanning transmission X-ray microscope enable spatially resolved analysis of magnetic domains and chemical composition. These examples illustrate DEMETER's capability for probing magnetic order and nanostructure with high spatial and spectral resolution. The beamline, operated in collaboration with the Jerzy Haber Institute of Catalysis and Surface Chemistry of the Polish Academy of Sciences and the AGH University of Science and Technology, provides a versatile platform for advanced research in nanoscience and magnetism.

topics: synchrotron, microscopy, X-ray, magnetism

1. Introduction

Magnetic materials and nanoscale surface phenomena play a central role in a wide array of contemporary technologies, from spintronics [1–3] to catalysis [4, 5] and quantum materials [6, 7]. The ability to probe magnetic order, domain structures, and chemical heterogeneity with high spatial and energetic resolution is essential for understanding and engineering these complex systems. The DEMETER beamline at the SOLARIS synchrotron has been purpose-built to meet these demands, offering state-of-the-art experimental capabilities for surface-sensitive imaging and spectroscopy using soft X-rays.

At the heart of the DEMETER beamline is an elliptically polarizing undulator (EPU), which delivers high-brightness, variable-polarization radiation across a wide energy range (100–2000 eV). This allows for resonant excitation at absorption edges relevant for chemical and magnetic contrast, such as those of 3d transition metals and rare-earth elements. The beamline comprises two end-stations, which are tailored to different yet complementary measurement strategies. The first system, a spectroscopic photoemission and low-energy electron microscope (SPELEEM), integrates a photoemission electron microscope (PEEM) with a low-energy electron microscope (LEEM) [8, 9], enabling real-time imaging of nanostructured surfaces over a wide temperature range (from –160°C to 1200°C).

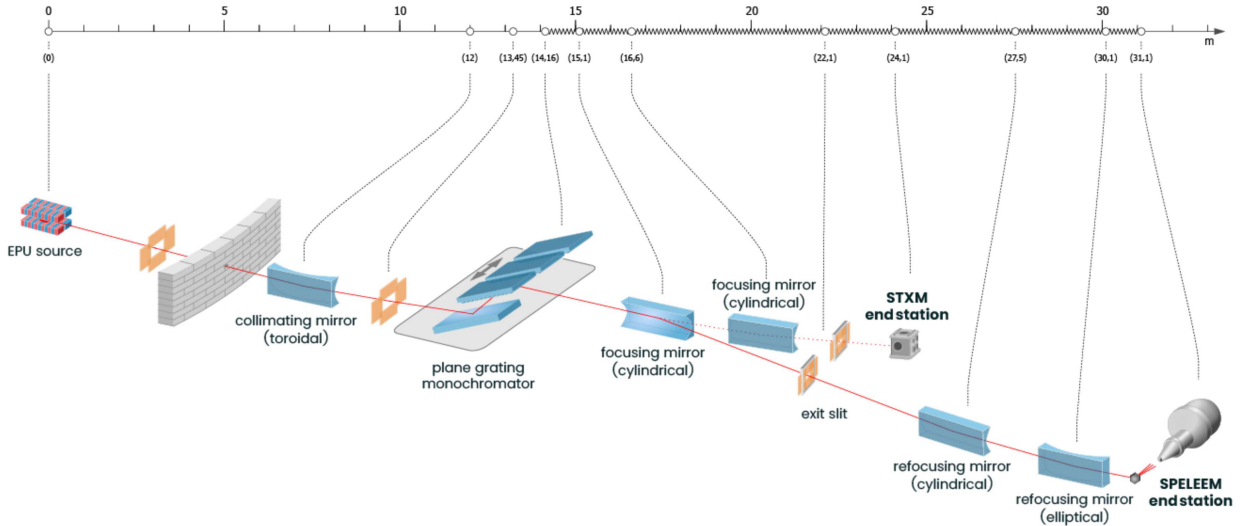


Fig. 1. General layout of the DEMETER beamline.

The second system, a scanning transmission X-ray microscope (STXM), enables high-resolution chemical mapping in transmission mode with advanced detection schemes [10].

The DEMETER beamline operates as a part of a collaboration between the Jerzy Haber Institute of Catalysis and Surface Chemistry of the Polish Academy of Sciences and the AGH University of Science and Technology. This partnership not only ensures the continuous development and expert operation of the beamline but also offers users access to complementary analytical tools, such as magnetotransport and magneto-optical measurements under extreme conditions. Together, the infrastructure and scientific support provided by DEMETER establish it as a unique and powerful tool for exploring magnetic phenomena and materials at the nanoscale with unparalleled precision.

2. DEMETER beamline

The DEMETER beamline is partly a “second-hand” installation, as several of its optical components originate from the former I1011 beamline at MAX II — specifically, the undulator, monochromator, and toroidal and cylindrical mirrors. After being transferred to SOLARIS, these elements were refurbished, optical elements were repolished, and integrated into the DEMETER beamline [11]. At present, DEMETER is the only beamline at SOLARIS equipped with two independent branches serving two experimental end-stations [12]. A schematic overview of the beamline is shown in Fig. 1.

The synchrotron radiation for the DEMETER beamline is generated by an elliptically polarizing undulator (EPU) installed in the storage ring. This

device delivers soft X-rays across a broad energy range (100–2000 eV) with variable polarization — linear (vertical and horizontal), circular, or elliptical — achieved by adjusting the phase of its magnet sub-girders. Such flexibility is especially valuable for X-ray magnetic dichroism and other element-specific techniques, allowing sensitive probing of magnetic and electronic properties in both bulk and nanoscale materials.

The EPU has a total length of 2.14 m and a period length of 46.6 mm. Its high photon flux enables measurements on dilute magnetic samples and nanostructures. The third harmonic of the undulator radiation covers the full range of L edges of the 3d transition-metal series, providing direct access to technologically important materials.

After leaving the undulator, the first optical element in the experimental hall is a toroidal collimating mirror that minimizes astigmatism, collimates the beam for the monochromator optics, and focuses the beam horizontally at the position of the exit slits. Next comes a collimated plane grating monochromator (cPGM), consisting of a plane mirror and three exchangeable diffraction gratings (i.e., 336, 1221, or 1400 l/mm). This setup preserves the polarization state while providing precise energy selection anywhere within the 100–2000 eV range. By balancing the monochromator parameters, the beamline achieves a resolving power of about 8000 with flux at the sample of roughly 10^{11} photons/s.

Downstream, cylindrical focusing mirrors direct the beam toward one of two experimental stations, namely a photoemission electron microscope branch or a scanning transmission X-ray microscope branch. Only one branch receives the photon beam at a time, and the optical configuration is adjusted accordingly to maintain high flux and resolution at the sample position. Additionally, for

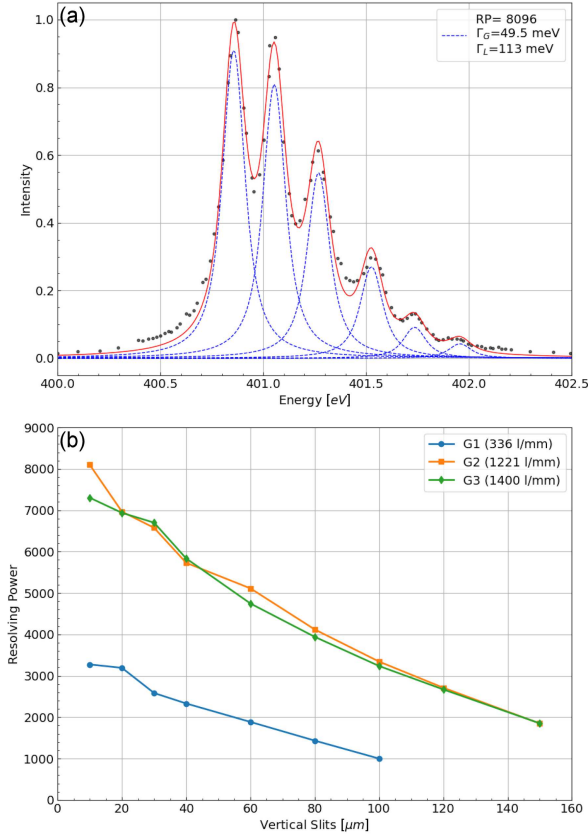


Fig. 2. Measured N_2 gas spectrum at the N K edge, with an exit slit opening of $10 \mu\text{m}$ and $\text{cff} = 2.25$ (a). Dependence of the resolving power on the slit size for each grating (b).

the SPELEEM end-station, a Kirkpatrick–Baez refocusing optics is installed to improve the mainly horizontal beam spot at the sample position.

Both experimental branches are equipped with vertical and horizontal exit slits, enabling independent control of beam size and energy resolution. The maximum illuminated area on the sample can reach $100 \times 300 \mu\text{m}^2$ or $300 \mu\text{m}$ in diameter, allowing for experiments ranging from high-resolution imaging to spatially averaged measurements. To evaluate the energy-resolving power, X-ray absorption spectra (XAS) of different gases were recorded using a gas cell permanently installed in the beamline directly after the exit slit. Figure 2a shows the nitrogen K edge spectrum of N_2 , corresponding to the N $1s \rightarrow \pi$ transition near 400 eV. The measurement was carried out with $\text{cff} = 2.25$ and an exit slit width of $10 \mu\text{m}$. The absorption peaks were modeled using Voigt profiles, obtained from the convolution of a Lorentzian function (representing the finite lifetime of the N $1s$ core hole) and a Gaussian function (representing the instrumental energy bandwidth). The spectrum was fitted with six Voigt functions, where the lifetime broadening was fixed at 112 meV, consistent with the values reported in the literature [13]. From the fit, a Gaussian full width at half

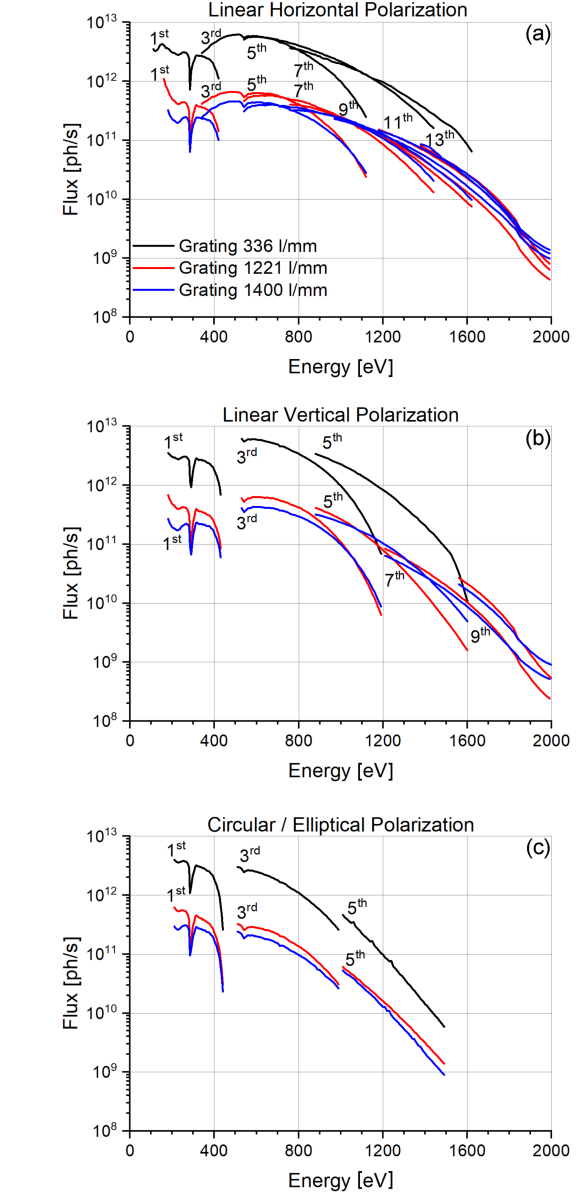


Fig. 3. Flux measured at the sample position for (a–c) different polarization settings and harmonics.

maximum (FWHM) of 50 meV was extracted, yielding a resolving power of $400 \text{ eV} / 50 \text{ meV} \approx 8000$. The measured N_2 gas spectrum and the dependence of the resolving power on the slit size for each grating are shown in Fig. 2b.

The photon flux at the sample position, measured with an absolute extreme ultraviolet (AXUV) photodiode, reaches values of 10^9 – 10^{12} photons/s under typical operating conditions (400 mA storage ring current, $40 \mu\text{m}$ exit slit, and optimized cff for each grating: 336, 1221, and 1400 l/mm); see Fig. 3. The combination of high flux, tunable polarization, and broad energy control makes DEMETER a versatile and powerful instrument for nanoscale studies of element-specific magnetic and electronic structures [14].

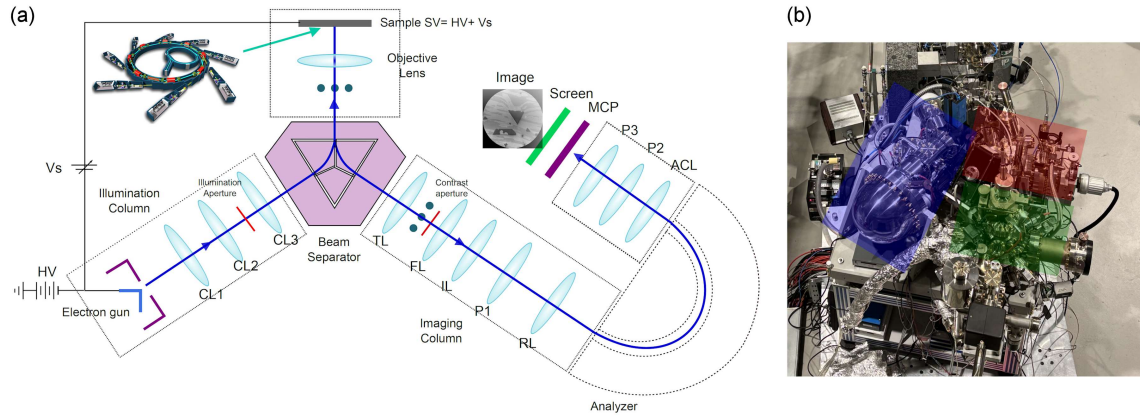


Fig. 4. (a) Schematic drawing of the SPELEEM setup. (b) Photo of the SPELEEM microscope installed at the DEMETER beamline. The colors indicate the most important parts of the microscope: green — preparation chamber (PCH), red — main chamber (MCH) with objective lens and sample, and blue — illumination and imaging column (COL).

2.1. Photoemission electron microscopy (PEEM)

Photoemission electron microscopy (PEEM) is a high-resolution imaging and spectroscopic technique that provides unique insight into the surface morphology, electronic structure, chemical composition, and magnetic properties of materials at the nanometer scale. It has become a key tool for studying magnetic thin films, nanoscale structures, and spin textures, particularly in the context of functional materials and nanomagnetism [8, 9, 15].

Operating within the framework of cathode lens microscopy, PEEM uses the sample surface as the electron emitter under soft X-ray illumination. The emitted low-energy electrons are accelerated and guided through an electron optical column before being projected as an image onto a detector system. This setup enables the combination of high spatial, energy, and angular resolution, making it possible to directly visualize nanoscale processes and correlate them with electronic and magnetic properties.

A defining strength of PEEM lies in its ability to provide element-specific magnetic contrast using polarized synchrotron radiation. Techniques such as X-ray magnetic circular dichroism (XMCD) and X-ray magnetic linear dichroism (XMLD) allow researchers to directly image ferromagnetic and antiferromagnetic domains, respectively, with nanometer precision. Beyond magnetism, PEEM also enables microspectroscopy and micro-diffraction, linking real-space imaging with detailed information about local electronic structure and crystallography.

Since 2023, the instrument has been further expanded with an electron gun and beam separator, enabling low-energy electron microscopy (LEEM). This complementary mode allows for topographic and structural imaging of surfaces, thin films, and interfaces, broadening the scope of investigations

beyond photon-induced processes [16, 17]. The current layout of the microscope and its location at the DEMETER beamline are shown in Fig. 4.

By combining imaging, spectroscopy, and diffraction in a single platform, PEEM offers a uniquely powerful approach to exploring the interplay between structure, chemistry, and magnetism at the nanoscale. Its versatility makes it indispensable for research in spintronics, correlated electron systems, and advanced functional materials.

2.2. Scanning transmission X-ray microscope (STXM)

The second end-station installed at the separate branch of the DEMETER beamline is a scanning transmission X-ray microscope, which produces microscopic images of samples by raster-scanning them and detecting the intensity of transmitted X-rays.

A central element of the microscope is the Fresnel zone plate — a diffractive lens that focuses the monochromatic X-ray beam. An aperture blocks unwanted diffraction orders, while the sample is placed in the lens focus and scanned with high precision using a piezoelectric stage. The transmitted X-rays are usually detected with a fast photodiode or with a more sensitive photomultiplier when signals are weak. The general layout and central part of the STXM are presented in Fig. 5.

Because soft X-rays are absorbed in air, the microscope operates in a vacuum. For delicate samples, a helium atmosphere or thin membrane enclosures can be used. Samples must be of suitable thickness to provide measurable absorption contrast and are often prepared on silicon nitride membranes or electron microscopy grids, or thinned with microtomy or focused ion beam techniques [10, 18].

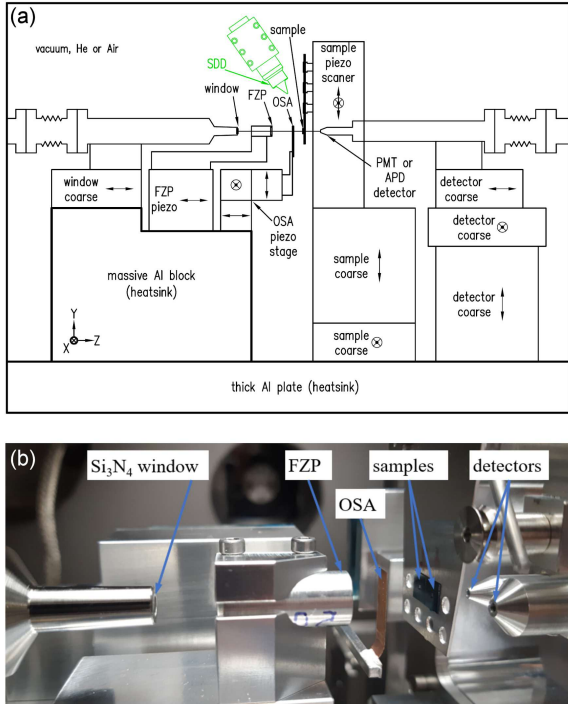


Fig. 5. (a) Schematic drawing of the STXM setup. (b) Inner part of the STXM microscope installed at the DEMETER beamline.

The spatial resolution typically ranges from 20 to 100 nanometers, limited by the focusing properties of the Fresnel lens. One key measurement mode is the “image stack,” where images are collected across a range of photon energies. This allows for the extraction of local absorption spectra and detailed chemical mapping at the nanoscale.

An additional advantage of the microscope is the ability to use variable polarization of the synchrotron beam, enabling magnetic contrast imaging through techniques such as X-ray magnetic circular dichroism. For example, magnetic domains in thin Nd–Fe–B layers can be visualized by comparing images taken with left- and right-circularly polarized light.

3. Results

3.1. Magnetic imaging using PEEM

To highlight the capabilities of the photoemission electron microscope (PEEM) at the DEMETER beamline, a series of experiments was carried out on magnetic materials. Since PEEM is an emission-based technique, it imposes specific requirements on sample properties — a conductive surface is essential to allow for efficient photoelectron emission and stable imaging conditions. Insulating samples typically require the addition of a conductive coating to prevent charging effects.

The modification of the interfacial magnetic structure in the oxidic heterosystem $\text{Fe}_3\text{O}_4/\text{NiO}$ is of considerable interest due to the contrasting electronic and magnetic properties of the two oxides. Fe_3O_4 is a ferrimagnetic half-metal with a high Curie temperature (858 K), while NiO is a prototypical antiferromagnetic insulator. Their interface provides a model system for exploring exchange coupling, spin alignment, and proximity-induced effects, which are relevant for spintronic applications. Notably, the $\text{Fe}_3\text{O}_4(001)$ surface has been widely investigated in the past and is known to exhibit a well-defined surface reconstruction, making it a reliable template for epitaxial NiO growth.

3.1.1. Prior studies on $\text{Fe}_3\text{O}_4(001)/\text{NiO}$

Several studies have explored the structural and magnetic properties of NiO films grown on $\text{Fe}_3\text{O}_4(001)$ [19–21]. Early work demonstrated that ultrathin NiO adopts the in-plane lattice symmetry of the magnetite substrate, leading to epitaxial strain that influences the orientation of the antiferromagnetic spin axis [22]. X-ray dichroism measurements revealed the presence of uncompensated Ni spins at the interface, which couple to the ferrimagnetic Fe_3O_4 and contribute to the exchange bias phenomena [23]. More recent investigations have focused on the role of finite-size effects in NiO, showing that the thickness-dependent stabilization of antiferromagnetic domains is strongly influenced by the magnetite substrate [20]. Together, these studies establish $\text{Fe}_3\text{O}_4(001)/\text{NiO}$ as a prototypical system for investigating the interplay of strain, symmetry, and interfacial exchange interactions in oxide heterostructures.

3.1.2. Sample preparation

Synthetic single crystals of magnetite (Fe_3O_4), oriented and polished to expose the (001) surface, were used as substrates. To achieve a stoichiometric and well-ordered template, the substrates were prepared closely following established procedures [24], which involve repeated cycles of Ar^+ ion sputtering (1 keV) and annealing in an oxygen atmosphere (10^{-6} mbar) at 900–1100 K. Consistent with earlier study [25], this treatment yields a characteristic surface reconstruction associated with a surface termination that alternates between octahedral (B) and tetrahedral (A) sites. The structural and electronic quality of the surface was verified in situ by X-ray absorption spectroscopy and X-ray magnetic circular and linear dichroism. The stoichiometry was assessed by comparing the experimental spectra with multiplet calculations of Fe^{2+} and Fe^{3+} in tetrahedral and octahedral coordination, using the Fe L_3 region,

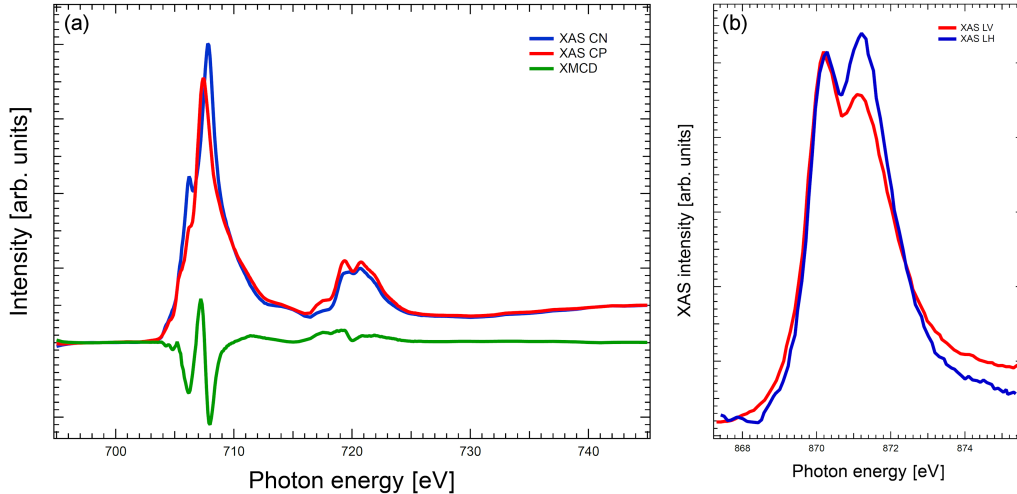


Fig. 6. (a) X-ray absorption spectra recorded at the Fe $L_{3,2}$ edges with opposite circular polarizations. (b) Microspectrum at the Ni L_2 edge measured with linearly polarized photons with horizontal and vertical polarization.

where the agreement is typically most reliable [26]. In Fig. 6a, the spectra of Fe $L_{3,2}$ taken with opposite circular polarizations are shown. The characteristic three-peak structure is quite clear in the XMCD signal, which confirms the stoichiometric character of the surface.

Subsequently, NiO was deposited by molecular beam epitaxy (MBE) at room temperature at an oxygen background pressure of 10^{-6} mbar. The molecular beam was directed perpendicular to the surface in order to minimize deposition-induced anisotropies. To stabilize the antiferromagnetic domain state of NiO, the sample was heated to 573 K after deposition, i.e., above the bulk Néel temperature of NiO (523 K). The magnetic ordering of NiO strongly depends on film thickness; ultrathin films, such as a single monolayer on Ag(100), have been reported to exhibit antiferromagnetism only well below room temperature, whereas thicker layers can sustain it at ambient conditions [27]. In the present work, we deposited 10 monolayers of NiO, ensuring — based on previous studies by Krug et al. [19] — that a pronounced magnetic contrast is obtained. To directly probe the antiferromagnetic character of our films, we performed XAS microspectroscopy at the Ni L_2 edge. The spectra shown in Fig. 6b exhibit the characteristic double-peak structure; importantly, for both polarizations, the intensity ratio between the first and second peak deviates from unity, providing clear evidence of the presence of a magnetic signal at the surface [19, 20].

To elucidate the magnetic domain structure, we acquired XMCD-PEEM images for each component using both circular and linear polarization. The images were recorded at the energy of the first maximum of the Fe XMCD spectrum, where the magnetic contrast is the strongest. At the Ni edge, XMCD was measured at the L_3 edge, while XMLD

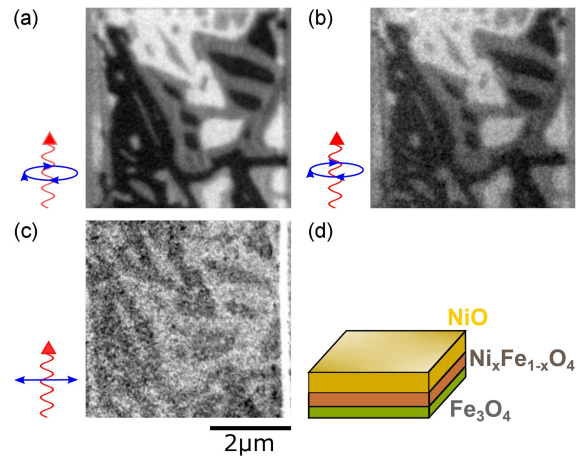


Fig. 7. (a) XMCD-PEEM image of the $\text{Fe}_3\text{O}_4(001)$ surface acquired at Fe L_3 edge. (b) XMCD-PEEM image at the Ni L_3 edge. (c) XMLD-PEEM image taken with linear vertical polarization at two energies corresponding to two peaks at the Ni L_2 edge. (d) Schematic drawing of the studied system.

images were collected at two energies corresponding to the two peaks of the Ni L_2 edge and combined to obtain the dichroic signal. The Ni XMCD contrast closely mirrors that of Fe, indicating strong coupling between Ni and Fe moments at the interface. This suggests that interfacial mixing or hybridization mediates exchange interactions across the NiO/ Fe_3O_4 boundary. As shown in Fig. 7, the (001) surface of magnetite exhibits its characteristic rib-like domain morphology, with elongated domains running along the crystallographic directions and forming a stable, labyrinthine network.

3.2. Magnetism in STXM

Although a scanning transmission X-ray microscope (STXM) at the beamline is not fully dedicated to magnetic studies, it is nonetheless capable of imaging the magnetic domains. The main constraint is the sample thickness, which must be suitable to ensure sufficient beam transmission. For transition-metal edges (600–1000 eV), this typically corresponds to thicknesses of only a few tens of micrometres. One of the main advantages of STXM is

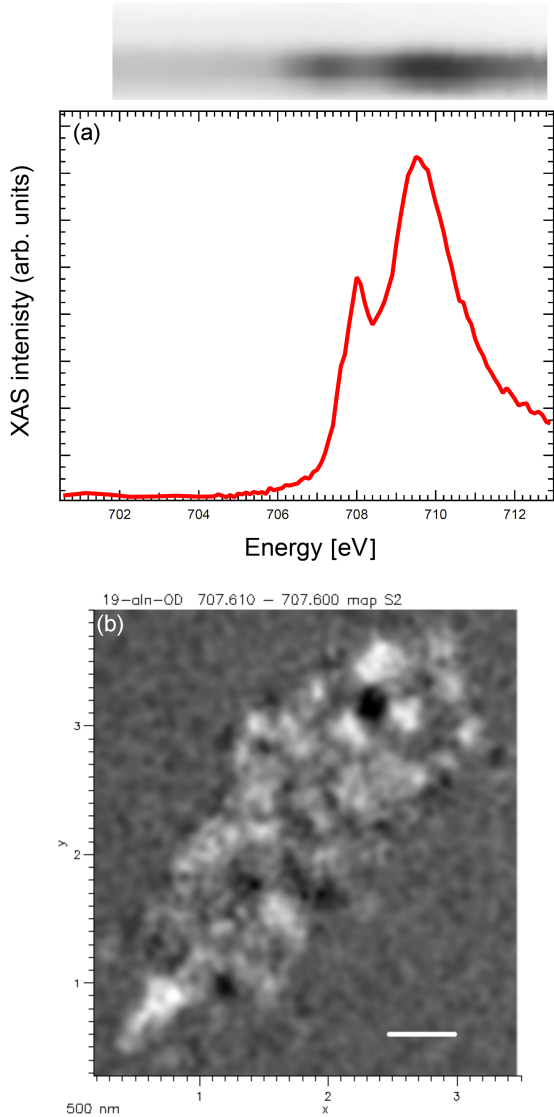


Fig. 8. (a) Absorption line scan (top) and corresponding absorption spectra (bottom) from the single-domain area marked in panel (b). (b) XMCD-STXM image of the SFO nanodots measured at the Fe L_3 edge (707.6 eV). This image was obtained by subtracting two optical-density (OD) images acquired with opposite photon polarizations.

that it fills the gap left by PEEM due to geometric limitations. In PEEM, the nearly grazing-incidence geometry makes the technique more sensitive to in-plane magnetic contrast. In STXM, the beam impinges at normal incidence, making it sensitive to out-of-plane magnetic contrast and therefore particularly well suited for studying samples with perpendicular magnetic anisotropy (e.g., skyrmions). At present, magnetic samples can only be studied in remanence, as there is no possibility to apply a magnetic field in situ. In the future, we plan to extend the capabilities of STXM by installing a rotatable sample stage to investigate in-plane magnetic domain distributions at different angles, as well as a magnetic coil for in-situ magnetic-field applications.

As an example of STXM application, we have investigated strontium hexaferrite ($\text{SrFe}_{12}\text{O}_{19}$, SFO) nanoparticles exhibiting perpendicular magnetic anisotropy. Samples consisted of nanoparticles with diameters ranging from ≈ 2 to 50 nm. For these measurements, the particles were dispersed in ethanol and deposited on commercially available silicon nitride membranes, which provide ideal support for transmission studies of this type. The STXM sample holder accommodates up to seven specimens simultaneously within the microscope chamber; in this study, three different nanoparticle size fractions were mounted side by side to enable direct comparison of their magnetic behavior. In addition to high-resolution imaging, the STXM setup also enables acquisition of X-ray absorption spectra from selected points of interest. For example, XAS spectra at the Fe L_3 edge were recorded from single locations on the sample to verify the photon-energy calibration and to assess the local chemical state prior to imaging. Figure 8a presents a partial XAS spectrum for one helicity of the synchrotron light, revealing the characteristic Fe L_3 double-peak structure typical of SFO. To obtain the XMCD-STXM image, two images with opposite helicities were acquired at the energy corresponding to the first peak of the L_3 edge (determined from reference data). The obtained dichroic image (Fig. 8b) exhibits clear magnetic contrast from the SFO nanoparticles [28, 29], demonstrating the sensitivity of this technique even with the present limitations.

The spatial resolution in these measurements was determined by the Fresnel zone plate used in the experiment, which provided a nominal resolution of ≈ 25 nm (equivalent to roughly 2–3 pixels spanning this distance). Although the current STXM configuration imposes certain constraints on magnetic measurements, these results indicate its potential for nanoscale magnetic imaging. Planned upgrades — including improved optics, rotatable sample stages, and in-situ magnetic-field capabilities — are expected to significantly extend the performance of the microscope and broaden the appeal to a wider user community.

4. Conclusions

The DEMETER beamline at the SOLARIS synchrotron provides complementary surface-sensitive and transmission-mode soft X-ray microscopes for element-specific imaging and spectroscopy of magnetic and electronic structures. Using PEEM, we demonstrated high-resolution visualization of magnetic domains and extraction of quantitative parameters such as domain wall widths in oxide heterostructures. With STXM, single-point XAS at the Fe L₃ edge verified photon-energy calibration and chemical state, while XMCD-STXM images revealed clear out-of-plane magnetic contrast from SrFe₁₂O₁₉ nanoparticles at a nominal spatial resolution of 25 nm. Although STXM currently operates only in remanence, planned upgrades (a rotatable stage and in-situ magnetic-field capabilities) will expand its functionality. Together, these features establish DEMETER as a versatile and powerful platform for nanoscale studies of magnetic materials and surface phenomena.

Acknowledgments

The authors gratefully acknowledge the invaluable support of all the beamline scientists involved in this project for their expertise and dedication. We are also deeply indebted to the research group of Professor Nika Spiridis and to our colleagues from the AGH University for their continuous collaboration and insightful contributions throughout the work. In particular, we wish to express our special gratitude to Doctor Tolek Tyliczszak for his outstanding assistance during the installation and commissioning of the beamline, which was crucial to the success of this effort. We also extend our sincere thanks to Professor Józef Korecki for his valuable insights regarding the PEEM setup and for establishing the PEEM/XAS agreement, which enabled the installation of the microscope at the SOLARIS synchrotron. Research at the National Synchrotron Radiation Centre SOLARIS is supported by the Ministry of Science and Higher Education, Poland, under contract no. 1/SOL/2021/2.

References

- [1] A. Hirohata, H. Sukegawa, H. Yanagihara, I. Žutić, T. Seki, S. Mizukam, R. Swaminathan, *IEEE Trans. Magn.* **51**, 0800511 (2015).
- [2] S.N. Kajale, J. Hanna, K. Jang, D. Sarkar, *Nano Res.* **17**, 743 (2024).
- [3] Y. Xie, S.-Y. Zhang, Y. Yin, N. Zheng, A. Ali, M. Younis, S. Ruan, Y.-J. Zeng, *npj Spintron.* **3**, 10 (2025).
- [4] Q. Zhang, X. Yang, J. Guan, *ACS Appl. Nano Mater.* **2**, 4681 (2019).
- [5] L.M. Rossi, N.J.S. Costa, F.P. Silva, R. Wojcieszak, *Green Chem.* **16**, 2906 (2014).
- [6] M. Liu, Y. Ye, J. Ye, T. Gao, D. Wang, G. Chen, Z. Song, *Magnetochemistry* **9**, 110 (2023).
- [7] A. Grubišić-Čabo, M.H.D. Guimarães, D. Afanasiev, J.H. Garcia Aguilar, I. Aguilera, M.N. Ali, S. Bhattacharyya, Y.M. Blanter, R. Bosma, Z. Cheng, *2D Mater.* **12**, 031501 (2025).
- [8] T. Schmidt, S. Heun, J. Slezak, J. Diaz, K.C. Prince, G. Lilienkamp, E. Bauer, *Surf. Rev. Lett.* **05**, 1287 (1998).
- [9] A. Locatelli, L. Aballe, T.O. Mendes, M. Kiskinova, E. Bauer, *Surf. Interface Anal.* **38**, 1554 (2006).
- [10] K. Benzerara, T.H. Yoon, T. Tyliczszak, B. Constantz, A.M. Spormann, G.E. Brown Jr., *Geobiology* **2**, 249 (2004).
- [11] I.A. Kowalik, G. Öhrwall, B.N. Jensen, R. Sankari, E. Wallén, U. Johansson, O. Karis, D. Arvanitis, *J. Phys. Conf. Ser.* **211**, 012030 (2010).
- [12] J. Szlachetko, J. Szade, E. Beyer et al., *Eur. Phys. J. Plus* **138**, 10 (2023).
- [13] C. Piamonteze, U. Flechsig, S. Rusponi et al., *J. Synchrotron Radiat.* **19**, 661 (2012).
- [14] V.N. Strocov, T. Schmitt, U. Flechsig et al., *J. Synchrotron Radiat.* **17**, 631 (2010).
- [15] J. Feng, A. Scholl, in: *Science of Microscopy*, Eds. P.W. Hawkes, J.C.H. Spence, Springer New York, 2006 p. 657.
- [16] E. Bauer, *Rep. Prog. Phys.* **57**, 895 (1994).
- [17] E. Bauer, *J. Electron Spectrosc. Relat. Phenom.* **241**, 146806 (2020).
- [18] A.L.D. Kilcoyne, T. Tyliczszak, W.F. Steele et al., *J. Synchrotron Radiat.* **10**, 125 (2003).
- [19] I.P. Krug, F.U. Hillebrecht, H. Gomonaj, M.W. Haverkort, A. Tanaka, L.H. Tjeng, C.M. Schneider, *Europhys. Lett.* **81**, 17005 (2007).
- [20] I.P. Krug, F.U. Hillebrecht, M.W. Haverkort et al., *Phys. Rev. B* **78**, 064427 (2008).

- [21] M. Finazzi, A. Brambilla, L. Duó, G. Ghiringhelli, M. Portalupi, F. Ciccacci, M. Zaccagna M. Zangrando, *Phys. Rev. B* **70**, 235420 (2004).
- [22] C. Giovanardi, A. di Bona, S. Altieri, P. Luches, M. Liberati, F. Rossi, S. Valeri, *Thin Solid Films* **428**, 195 (2003).
- [23] J. Nogués, I.K. Schuller, *J. Magn. Magn. Mater.* **192**, 203 (1999).
- [24] L. Martín-García, R. Gargallo-Caballero, M. Monti, M. Foerster, J.F. Marco, L. Aballe, J. de la Figuera, *Phys. Rev. B* **91**, 020408(R) (2015).
- [25] E. Goering, S. Gold, M. Lafkioti, G. Schütz, *Europhys. Lett.* **73**, 97 (2006).
- [26] M. Monti, B. Santos, A. Mascaraque et al. *Phys. Rev. B* **85**, 020404(R) (2012).
- [27] M.W. Haverkort, S.I. Csiszar, Z. Hu et al., *Phys. Rev. B* **69**, 020408(R) (2004).
- [28] G.D. Soria, C. Granados-Miralles, A. Mandziak et al., *J. Phys. D* **54**, 054003 (2020).
- [29] G.D. Soria, J.F. Marco, A. Mandziak et al., *J. Phys. D* **53**, 344002 (2020).